



Original article

2D- and 3D-QSAR of Tocainide and Mexiletine analogues acting as Na_v1.4 channel blockers

Antonio Carrieri*, Marilena Muraglia, Filomena Corbo, Concetta Pacifico

Dipartimento Farmaco-Chimico, Università degli Studi di Bari, via Orabona 4, 70125 Bari, Italy

ARTICLE INFO

Article history:

Received 12 March 2008

Received in revised form

30 June 2008

Accepted 1 October 2008

Available online 14 October 2008

Keywords:

3D-QSAR

GRIND

Tocainide

Mexiletine

Sodium channel

ABSTRACT

Enantiomeric forms of Tocainide, Mexiletine, and structurally related local anaesthetic compounds, were analyzed with respect to their potency in blocking Na_v1.4 channel. Structure–activity relationships based on *in vitro* pharmacological assays, suggested that an increase in terms of lipophilicity and/or molecular surface as well as the presence of specific polar spacers might be determinant for receptor interactions. QSAR and pharmacophore models were then used to support at 3D level this hypothesis.

© 2008 Elsevier Masson SAS. All rights reserved.

1. Introduction

Ion channels blockers are powerful drugs in the treatment of several disorders generally characterized by abnormal membrane excitability (i.e. autoimmune disorders, hypertension, cardiac arrhythmias and heart failure, Alzheimer's and Parkinson's diseases and many others) [1].

Among the ion channels blockers the key role of the voltage-gated sodium channels (VGSCs) [2,3] is noteworthy. These channels play an important role in the neuronal network by transmitting electrical impulses rapidly throughout cells and cell network, thereby coordinating higher processes ranging from locomotion to cognition.

Sodium channels are heteromeric integral proteins, made up of two different subunits: an α -subunit, high in molecular weight and arranged in six transmembrane α -helices, that is part of a four domains' bundle spanning the cell membrane, and one or more β -subunits, with lower molecular weight, typically with a large extracellular N-terminal moiety resembling immunoglobulins. Within the fifth and the sixth helix of each domain a short non-helical segment highly rich in polar residues is located and site directed mutagenesis experiments have demonstrated that VGSCs binding site is located within this segment [4,5]. These channels might exist in three different states: resting, open and closed (or

inactivated). Membrane voltage governs ion channels cycling switch, which occurs at high frequency in the physiological channel types. Electrophysiological experiments proved that the resting to open blockade may be ranked by tonic block (TB) whereas the inactivated to resting by phasic block (PB) measurements. To address this topic it is important to have a state-dependent mechanism of inhibition.

A variety of VGSCs have been already identified by electrophysiological recording, biochemical purifications and molecular cloning [6] but the understanding of the structural mechanism of ion channels blocking [7], as well as the 3D characterization of the inactivated type, has been hampered by the paucity of robust information deriving either from X-ray or NMR data. In this restricted scenario the only way to gain insights into the structural requirements of these channels is therefore the derivation of ligand-based theoretical models capable of giving a better understanding and rationalization of biological data. This study would give an added value to the discovery of new compounds potentially useful in the treatment of diseases correlated to hyper-excitability of some tissues lacking the physiological phenotypes of sodium channels. As part of our ongoing program on the research of potent and selective sodium blockers, we previously focused our attention on the design and synthesis of compounds helpful to solve the myotonic syndromes, hereditary disorders of the skeletal muscle caused by missense mutations in the human skeletal muscle sodium channel isoform Na_v1.4 [8]. Unfortunately the sodium channel blockers nowadays clinically used to treat this disorder are not selective and therefore they have relatively narrow therapeutic

* Corresponding author. Tel.: +39 080 5442638; fax: +39 080 5442724.

E-mail address: carrieri@farmchim.uniba.it (A. Carrieri).

profile which might limit their usefulness and among different molecules known so far as VGSCs blockers, local anaesthetic including Tocainide (TOC) and Mexiletine (MEX) represent a promising class of compounds. Racemate mixture of MEX is nowadays used in therapy, although *in vitro* and *in vivo* assays highlighted a certain degree of stereoselectivity mainly in the cardiac tissue, being the (*R*)-(–)-enantiomer preferred over the (*S*)-(+)-one, but its side effects, especially on the central nervous system limit its wide use. On the other hand, TOC has a similar pharmacological and pharmacokinetic profile but it has even more pronounced side effects with respect to Mexiletine.

In the course of our synthesis program, TOC and MEX analogues, bearing different substituents on the phenyl ring as well as on the basic nitrogen, have been already synthesized [9–11] aiming to clarify the molecular determinants of local anaesthetic-like drugs and to find potent blockers, mostly selective towards Na_v1.4. These ligands have been pursued with respect to their ability to TB and PB block towards Na_v1.4, and the measured potency suggested a relevant role for lipophilicity and basicity for these compounds.

There have been several attempts to create SARs for this class of sodium channel blockers. Anyway the complexity on the target protein such as the way in which it changes in membrane potential held back the development of appropriate pharmacophore model. In order to achieve better clues on molecules' finger prints, a novel 3D-QSAR study was carried out by means of molecular descriptors capable of accurately ranking the measured activity, and a fresh pharmacophore hypothesis for local anaesthetic acting as VGSCs blockers is here proposed. In fact, very few molecular modeling studies have been published so far on this type of drugs [12,13] and they are likely aimed to depict the properties of sodium channels binding site by means of partial and theoretical models of the mere membrane moiety, but none of them have studied wide series of compounds and their potency values for VGSCs blocking.

In order to describe pharmacodynamic properties of TOC and MEX derivatives in their optically active forms, measured as PB, we make use of classical 2D- and advanced 3D-QSAR based on alignment independent descriptors: for the first time the efficacy is here quantitatively discussed and rationalized at 3D level, and a pharmacophore model for these compounds is proposed, aiming also to the establishment of a molecular tool able to predict VGSCs blocking for plausible new candidates targeting selectively Na_v1.4 sodium channel isoform in a use-dependent manner.

2. Methods

2.1. Chemistry

The synthesis, chemical characterization and the structure–activity relationships of compounds **1–23** reported in Table 1 have been previously described except for compound **2** that was synthesized according to the procedure described for compound **7** [8], and for compound **9** obtained by using synthetic pathways previously published [14].

Crystal structure of the racemic compound **8** was determined by X-ray diffraction method as reported in Section 5.

2.2. 2D-QSAR for VGSCs blocking

Regression models, showing the dependence of PB values on lipophilicity according to the bilinear approach reported by Kubinyi [15], and multiple regression analysis were generated with the program BILIN [16]. Lipophilic and basic molecular properties for VGSCs blocking activity were calculated as C Log *D* (pH = 7.42) and p*K*_a using the Advanced Chemistry Development (ACD) software [17].

2.3. 3D-QSAR for VGSCs blocking

Potency data were related to the recently introduced GRID independent descriptors (GRIND) [18]. They rely on the definition of a virtual binding site, and at the same time embody the geometrical relationship between hot spots of a receptor cavity.

Obtaining GRIND is a stepwise, but very quick and fully automated, procedure implying: (i) calculation at certain grid nodes of the molecular interaction fields (MIF) with properly selected atom probes by means of the program GRID [19]; (ii) filtering MIFs in order to extract the most salient chemical information regarding the receptor binding site; (iii) encoding the spatial relationship within the same binding site nodes into new 3D-independent variables multiplying the value of the interaction energy at each pair of node which is then handled according to the distance between them.

Correlograms obtained plotting node–node energy product vs euclidean distance between the same nodes allow the identification of variables most strongly affecting the pharmacodynamic properties of each molecule; at the same time the display of contoured MIFs helps the interpretation of biological data.

In our study four different probes, 1, DRY, 2, O, 3, N1, and 4, TIP, mimicking, respectively, the hydrophobic, hydrogen bond acceptor, hydrogen bond donor and molecular shape effects in the receptor–ligand interaction process were selected and four auto-correlograms (11, DRY–DRY; 22, O–O; 33, N1–N1; 44, TIP–TIP) and six cross-correlograms (12, DRY–O; 13, DRY–N1; 14, DRY–TIP; 23, O–N1; 24, O–TIP; 34, N1–TIP) were thus obtained.

GRIND, Principal Components Analysis (PCA) and Partial Least Squares (PLS) analysis were generated by ALMOND software (version 3.3.0) [20] using default settings (i.e. grid spacing, number of filtered nodes, percentage of field weight, etc.). No initial scaling was applied to the original X-variable matrix which was afterward filtered by one Fractional Factorial Design run.

Even though ALMOND results have proved to be not affected by likely unacceptable molecular superpositions [21], molecular fittings to X-ray structures of compound **8** were carried out, assuming that the conformation achieved in such a way might resemble most closely the bioactive one for the studied VGSCs blockers. Molecular structures form of protonated compounds **1–7** and **9–23**, built *via* Flo+ software [22] with standard bond distances and valence angles, were therefore flexibly superposed on each of the two conformations detected by X-ray diffraction on the racemic mixture of the highly PB active compound **8** through fifty thousand runs of the TFIT module implemented in the same software package.

Four different alignments, namely (*R*)-**A**, (*S*)-**A**, (*R*)-**B** and (*S*)-**B**, were afterwards generated and subsequently submitted to chemometric analyses choosing the conformation of each molecule having the best superposition energy, as scored by Flo+ was selected (see Table 2).

Crossvalidated analysis carried out using the Leave-One-Out (LOO) procedure was used to select the optimal number of component in the PLS models equal to a significant increase of the crossvalidation coefficient *q*² (at least 5%) and, as a rule of thumb, up to a dimensionality not more than one component for each five molecules.

3. Results and discussion

3.1. Crystallographic data

The structure of compound **8** was solved in the space group Cc and the asymmetric unit consists of two independent molecules (**A** and **B**). The two molecules **A** and **B** (Fig. 1) are reported, respectively, in *R* and *S* configuration, but space-group symmetry generates for any molecule its own enantiomer.

Table 1
Potency, clog *P* and basicity values for compounds **1–23**.

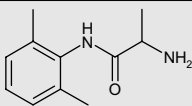
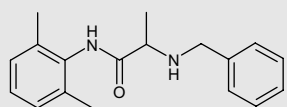
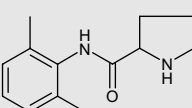
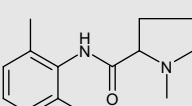
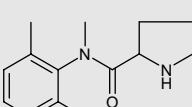
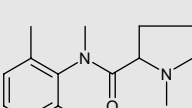
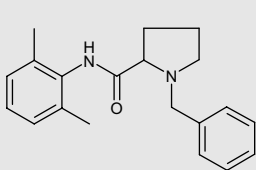
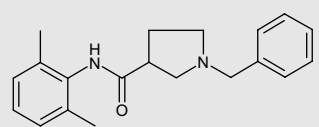
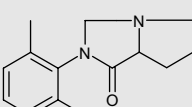
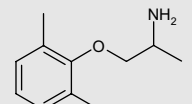
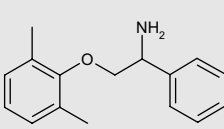
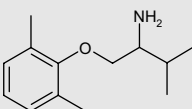
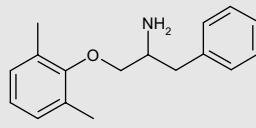
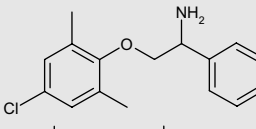
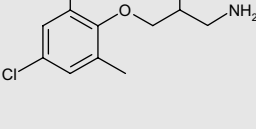
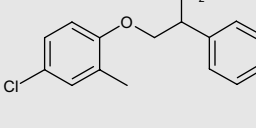
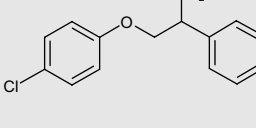
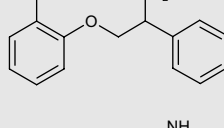
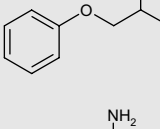
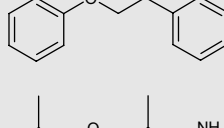
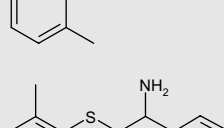
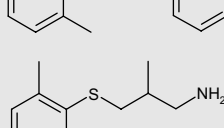
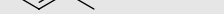
Compound		PB ^a	cLog <i>D</i> ^b	pK _a ^c	
TOC					
1		(<i>R</i>)	3.56	0.32	7.64
		(<i>S</i>)	3.65		
2		(<i>R</i>)	4.95	3.18	7.50
		(<i>S</i>)	5.04		
3		(<i>R</i>)	4.92	0.09	9.04
		(<i>S</i>)	4.39		
4		(<i>R</i>)	4.17	0.50	8.34
		(<i>S</i>)	4.55		
5		(<i>R</i>)	3.66	0.13	8.98
		(<i>S</i>)	4.17		
6		(<i>R</i>)	3.30	1.17	8.28
		(<i>S</i>)	3.70		
7		(<i>R</i>)	4.50	2.65	7.50
		(<i>S</i>)	5.00		
8		(<i>R</i>)	5.77	2.29	8.33
		(<i>S</i>)	5.64		
9		(<i>R</i>)	3.30	2.23	3.74
		(<i>S</i>)	nd		
MEX					
10		(<i>R</i>)	4.64	0.96	8.58
		(<i>S</i>)	4.57		
11		(<i>R</i>)	5.52	2.23	8.48
		(<i>S</i>)	5.52		
12		(<i>R</i>)	5.24	1.72	8.70
		(<i>S</i>)	5.24		

Table 1 (continued)

Compound		PB ^a	cLog <i>D</i> ^b	pK _a ^c	
13		(<i>R</i>)	5.62	3.28	7.84
		(<i>S</i>)	nd		
14		(<i>R</i>)	4.71	3.02	8.37
		(<i>S</i>)	5.10		
15		(<i>R</i>)	5.43	1.42	9.56
		(<i>S</i>)	5.54		
16		(<i>R</i>)	4.82	2.56	8.36
		(<i>S</i>)	4.64		
17		(<i>R</i>)	5.00	2.10	8.36
		(<i>S</i>)	5.52		
18		(<i>R</i>)	6.00	1.77	8.47
		(<i>S</i>)	5.52		
19		(<i>R</i>)	3.68	0.36	8.22
		(<i>S</i>)	3.63		
20		(<i>R</i>)	5.40	1.18	8.61
		(<i>S</i>)	4.80		
21		(<i>R</i>)	4.63	0.65	9.66
		(<i>S</i>)	4.76		
22		(<i>R</i>)	5.15	3.22	8.65
		(<i>S</i>)	5.33		
23		(<i>R</i>)	5.57	1.10	9.80
		(<i>S</i>)	5.72		

^a Tonic block pEC₅₀ (μM): block of sodium channel at resting state conditions evaluated during infrequent depolarizing pulses.^b Phasic block pEC₅₀ (μM): cumulative sodium current reduction by the drug at 10 Hz stimulation frequency, obtained by concentration–response curves.^c Calculated using Advanced Chemistry Development (ACD) Software [17].

Table 2

Statistical results of PLS analysis for PB potency data.

Model ^a	<i>n</i>	Variables ^b	<i>r</i> ^{2c}	<i>q</i> ^{2d}	SDEC ^e	ONC ^f
(<i>R</i>)- A	44	251	0.945	0.782	0.170	5
(<i>R</i>)- B	44	263	0.904	0.537	0.205	5
(<i>S</i>)- A	44	243	0.912	0.621	0.217	5
(<i>S</i>)- B	44	279	0.938	0.767	0.182	5

^a See text (Section 2).^b Selected via fractional factorial design.^c Correlation coefficient.^d Leave-one-out crossvalidated correlation coefficient.^e Standard error of the calculation.^f Optimal number of component according to the crossvalidation results.

The **A** molecule has a folder-shape, there is a short distance between a methyl group and the benzyl ring [C7A...C20A = 3.854(9) Å]. In the **B** molecule, that has extended molecular structure, the distance between the methyl group and the benzyl ring is longer [C7B...C20B = 9.801(9) Å].

In the crystal packing, the N–H...O hydrogen bonds link the *R* configuration **A** molecule with two adjacent *S* configured ones and vice versa [N1A...O1A(*x*, 1−*y*, *z* + 1/2) = 2.910(6) Å, (N1A)H1AN...O1A(*x*, 1−*y*, *z* + 1/2) = 2.06(6) Å, N1A–H1AN...O1A(*x*, 1−*y*, *z* + 1/2) = 166(4)°]; also *R* and *S* configuration **B** molecules are linked via N–H...O hydrogen bonds [N1B...O1B(*x*, 1−*y*, *z* + 1/2) = 2.870(5) Å, (N1B)H1BN...O1B(*x*, 1−*y*, *z* + 1/2) = 2.09(5) Å, N1B–H1BN...O1B(*x*, 1−*y*, *z* + 1/2) = 158(5)°]. As a result chains of **A** molecules and chains of **B** molecules extending along the *c* direction are formed.

3.2. Chemistry

As part of an ongoing program on the research of potent and selective Na⁺ channel blockers, we previously synthesized compounds **1–23** (Table 1) having partial structural analogy with the TOC and MEX, molecules capable of blocking the voltage-gated sodium channel [9,8,14].

The structure–activity relationships for this type of VGSCs blockers might be summarized as follows: in general TOC derivatives are less potent with respect to their MEX cognate indicating that the O–CH₂ spacer is better than the NH–CO one (e.g. compounds **1** vs **10**). For all the examined molecules potency and use-dependent behavior are strongly affected by the steric hindrance on the basic nitrogen since compounds with bulkier (i.e. benzyl) groups are the most active with respect to those bearing smaller substituents. In addition increasing the distance between the two aromatic rings seems to be crucial on the VGSC blocking activity (e.g. compounds **7** vs **8**).

Within the TOC derivatives the presence of hydrogen bonding groups is mandatory (e.g. compound **3** vs compound **4**, **5** and **9**) and β-prolinic ring is preferred over α-proline (e.g. compound **8** vs compound **7**).

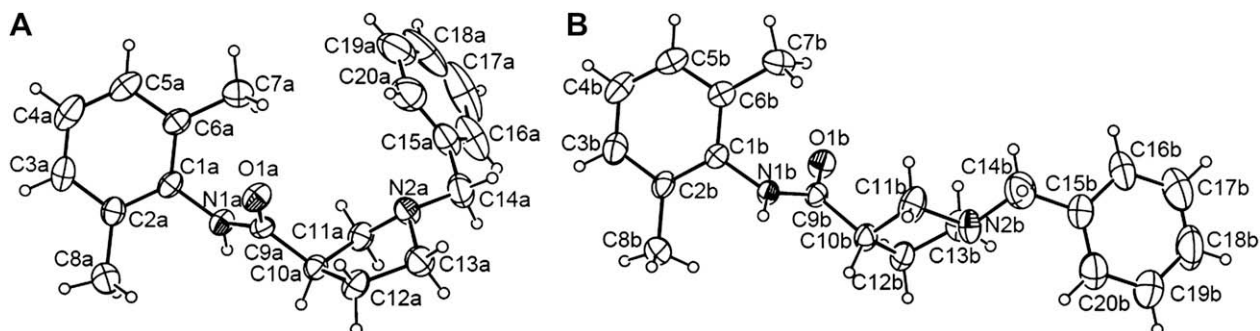


Fig. 1. ORTEP drawing of the independent molecules of compound **8**, the ellipsoids enclose 30% probability. (A) Molecule **A** is shown in *R* configuration, (B) molecule **B** is shown in *S* configuration.

By biological data reported in Table 1 it is evident that the increment in potency is independent of the substituents present on the aryloxy ring and, although less evident, it is conserved in phasic block experiments. However, the 4-chlorinated analogues (compound **14–17**) were generally less potent.

Finally no significant stereoselectivity was also observed being, for almost all enantiomers the eudismic ratio equal to 1.

3.3. 2D-QSAR

In order to rationale the evidences highlighted by SAR and to investigate the molecular determinants responsible for high PB profile, a 2D-QSAR study was carried out.

Interestingly, promising bilinear relationships between *C* Log *D* and pEC₅₀ of PB data for (*R*)- (Eq. (1)) and (*S*)- (Eq. (2)) enantiomers were obtained, where *n* is the number of compounds in correlation, *r*² the correlation coefficient, *s* the standard deviation and *F* the Fischer test, respectively.

$$\begin{aligned} \text{pEC}_{50} = & 3.174 (\pm 1.17) C \text{ Log } D \\ & - 3.629 (\pm 1.50) \log(\beta C \text{ Log } D + 1) \\ & + 3.161 (\pm 0.59) \log \beta \\ = & -0.905; n = 20; r^2 = 0.734; s = 0.402; F = 14.749 \end{aligned} \quad (1)$$

$$\begin{aligned} \text{pEC}_{50} = & 1.401 (\pm 0.62) C \text{ Log } D \\ & - 1.894 (\pm 1.08) \log(\beta C \text{ Log } D + 1) \\ & + 3.798 (\pm 0.46) \log \beta \\ = & -1.489; n = 20; r^2 = 0.666; s = 0.394; F = 10.632 \end{aligned} \quad (2)$$

Eq. (1) was achieved not including compounds (*R*)-**3**, (*R*)-**6** and (*R*)-**9**, while in Eq. (2) only (*R*)-**6** was deleted from the data set. The presence of these outliers might be justified according to an overestimation of *C* Log *D* value for compounds (*R*)-**6** and (*R*)-**9** and besides this it is worth noting that the aforementioned compounds are the lone lacking polar hydrogen. From a structural point of view, this might affect a highly congeneric series like the one we have examined. On the other hand it is rather unclear the reason why compound (*R*)-**3** does not fit PB data, but the presence of this outlier might be caused by its high PB/*C* Log *D* ratio, which very much exceeds the one calculated for the rest of the compounds.

As can be perceived from the PB vs *C* Log *D* plots reported in Fig. 2, non-linear dependence of PB data on lipophilicity might be elucidated by classical parabolic model as proposed by Hansch and Fujita [23] although account lower correlation coefficients (*r*² = 0.654 and *r*² = 0.641 for (*R*)- and (*S*)-, respectively), likewise better standard deviations are measured for bilinear regressions (*s* = 0.402 and 0.394 vs *s* = 0.445 and 0.397).

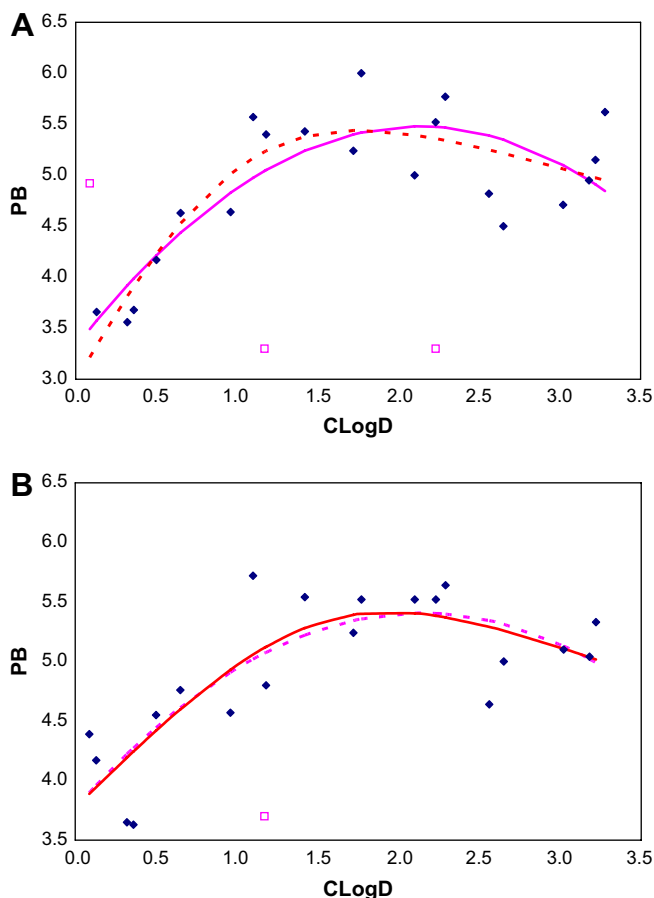


Fig. 2. Plot of PB vs CLogD data (top (R)-; bottom (S)- enantiomers). Solid and dashed lines represent the bilinear and parabolic regressions, respectively. Data not included in the regression models are represented by empty squares.

Enlarging the number of examined compounds and also the range of biological data might support further the Kubinyi's approach. In any case the substantial fitting of the Eqs. (1) and (2), while not outstanding, proves once again the role of lipophilicity as

important physicochemical property in the modulation of $\text{Na}_v1.4$ channel blocking activity.

Multivariate regression analysis next carried out with CLogD and pK_a variables support the dependence of PB by lipophilicity, and also basicity, of the examined compounds. For (R)- (Eq. (3)) and (S)- (Eq. (4)) enantiomers the following multiple regressions were obtained, with compound (S)-4 omitted as formerly:

$$\begin{aligned} \text{pEC}_{50} &= 0.465 (\pm 0.11) \text{C Log } D + 0.431 (\pm 0.10) \text{pK}_a \\ &\quad + 0.487 (\pm 0.89) \\ n &= 22; r^2 = 0.589; s = 0.514; F = 13.62 \end{aligned} \quad (3)$$

$$\begin{aligned} \text{pEC}_{50} &= 0.568 (\pm 0.10) \text{C Log } D + 0.616 (\pm 0.16) \text{pK}_a \\ &\quad - 1.286 (\pm 1.43) \\ n &= 20; r^2 = 0.677; s = 0.376; F = 17.83 \end{aligned} \quad (4)$$

Coefficients endowing positive values in Eqs. (3) and (4) for both CLogD and pK_a suggest that the two variables affect in the same way the biological profile of VGSCs blockers as already suggested by SAR.

These first preliminary results prompted us to go further into the $\text{Na}_v1.4$ channel binding site analysis, and to fulfill this topic, we decided to enlarge this study at 3D level, and possibly depict pharmacophore models explaining the structural properties of our molecules. All the synthesized compounds were taken into account with the exception of compounds (S)-9 and (S)-13 for which PB data have not been determined yet.

3.4. Phasic block chemometric analysis

GRIND descriptors calculated on the whole VGSC blockers set were analyzed through PCA in order to discriminate between structural motif and pharmacological profile characterizing these molecules. The two first components of the analysis were able to explain 50% of the structural variance. As can be perceived from the scores plot reported in Fig. 3 compounds are correctly distinguished according to their chemical nature by first component, being all the MEX derivatives clustered in the upper part while TOC analogues lay in the bottom part of the same plot. In addition to this, second

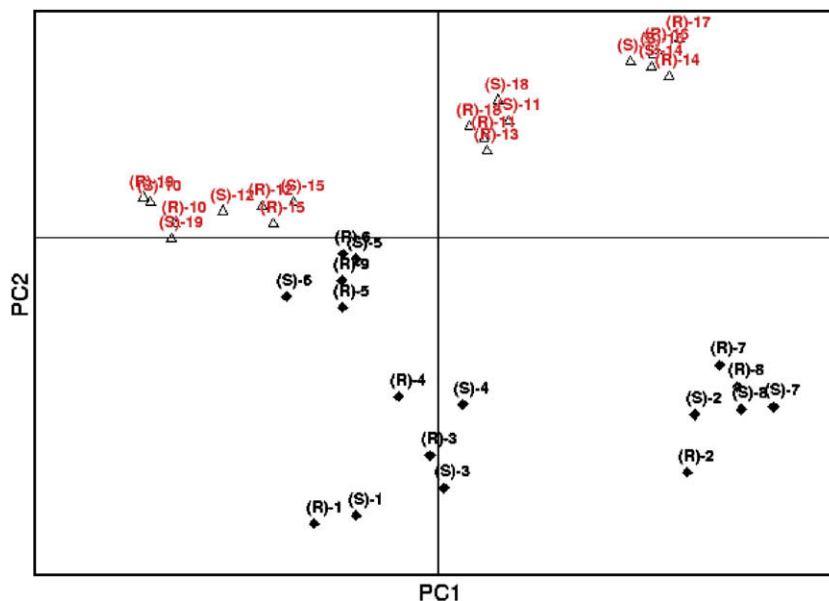


Fig. 3. PCA scores plot: TOC derivatives are represented by filled diamonds MEX by empty triangles. Highly active compounds are mainly placed on the right-hand side, low active on the left.

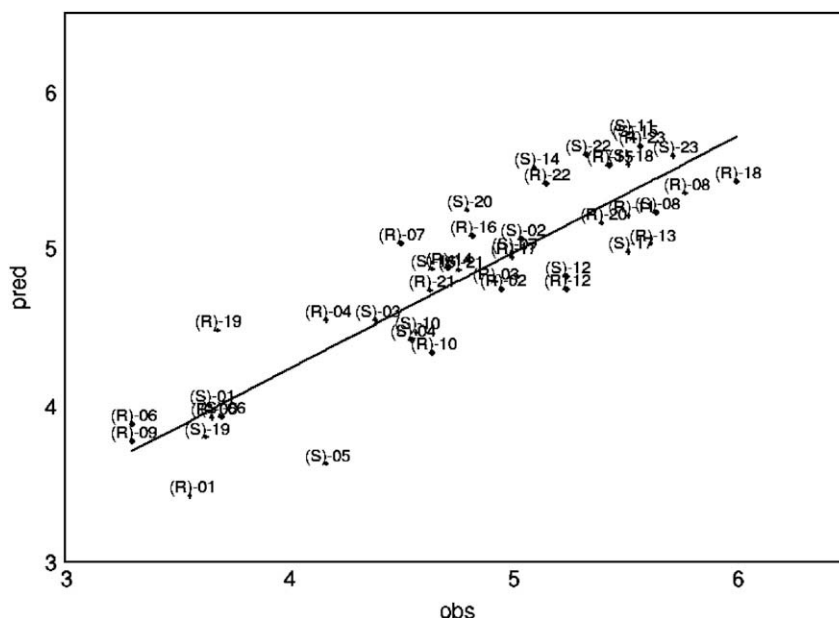


Fig. 4. Plot of experimental vs predicted PB data from the non-crossvalidated model (R)-A.

component groups VGSC blockers according to their potency with the most active compounds present in the right-hand quadrant and the less active one the left. Significantly and in agreement with the SAR no classification with respect to stereoisomerism is observed.

Afterwards the same GRIND descriptors were correlated with PB data by PLS multivariate analysis as reported in the Section 2.

From the statistical indices reported in Table 2 it can be noticed that, regardless of the molecular superpositions, sound models were obtained for the four different alignments, the percentage of explained variance being more than 90% in all of them. Likewise the valuable crossvalidated correlation coefficient removed the risk of false positive models obtained by chance correlation, all the q^2 being well above 0.3, which corresponds to a low probability of chance correlation ($p < 0.05$, that is $< 5\%$) [24].

It has to be pointed out that our chemometric analysis is based on the intramolecular distances resulted by the template fitting to crystallographic data of compounds **8** having, as reported in the before, two distinct conformations, folded and open. According to the mere statistics, all PLS models share very similar figures: the number of variables used, as well as correlation and crossvalidation coefficients, together with standard deviation of predictions and calculations, are greatly comparable. The same also applies to coefficients and weights of the PLS analysis, which gave similar plots, and then they are all capable of rationalizing the biological data. This evidence suggests that docking of these Na_v1.4 blockers might take place into a quite accessible and not so sterically hindered, foreseeing a better activity for molecules carrying on the basic moiety bigger substituents.

Merit of PLS analysis might also be perceived by the plot of experimental vs predicted data calculated from the highest r^2 model (R)-A where no significant outliers emerged (see Fig. 4).

Deeper insights into 3D-QSAR results might be gained from PLS coefficients which advise the chemical descriptors better describing an increase (positive coefficient) or decrease (negative coefficient) of activity (see Fig. 5). In detail, the magnitude and the positive coefficients of (R)-A PLS model suggested that molecular interaction fields measured at certain grid nodes and at a definite distance with TIP–TIP, DRY–O, DRY–TIP and O–TIP probes have the major impact on the PB potency, indeed variables 44–38, 12–30, 14–32 and 24–8 seemed to be the most relevant ones. Conversely

variable 24–36, 13–25, and with a less extent 44–42, are detrimental for affinity data as scored by their negative PLS coefficients. For the sake of clarity, the first two digits encode the used probe, the second numbers stand for distance between two favorably interacting nodes, and can be converted in Angstrom multiplying the number by the grid spacing and the smoothing window, 0.5 and 0.8 Å, respectively.

As weighted by ALMOND model for these VGSC blockers, two pharmacophoric elements emerged as the most salient, namely distance between molecule's edges (TIP–TIP), lipophilic centre and hydrogen bond donor atoms (DRY–O): the higher the distances between such nodes and more favorable the interaction energies measured with the aforementioned atoms probes, the better would be the resulting activity. On the contrary, distances between hydrophobic/aromatic group and hydrogen bond acceptor atom (DRY–N1) should be as lower as possible.

Shape effects seem to be more relevant since five out of the first ten variables with the higher coefficients are referred to TIP–TIP interactions, nonetheless hydrophobic forces combined with polar effect (i.e. DRY–O) are also crucial, three out of the first ten variables as well.

From the relative correlograms reported in Fig. 6 it can be observed that GRIND variable 44–38, endowing favorable TIP–TIP interactions occurring at longer distance, shows high values for PB potent compound (R)-**8**, while the same does not apply to weakly potent (R)-**1** where these interactions are totally absent. Similar indication might also be observed in the DRY–O correlogram where variables with high coefficients (i.e. 12–11 and 12–30) occupy the upper part of the plot for the most potent (R)-**8** molecule whereas weak compound (R)-**1** has less favorable interactions with the mentioned variables. A similar observation might be made of DRY–TIP variable 14–32 (data not shown). On the contrary variable 13–25, encoding a decrease of activity in terms of DRY–N1, is high for the same compound.

It is rather unclear the meaning of positive coefficients of variable 24–8 which might be partially explain the activity contribution for small, but low active, compounds.

Interestingly no information is gained by variables or auto-correlogram referred specifically to hydrogen bonding acceptor or donor interactions (i.e. O–O or N1–N1) and this might suggest that the nature of the bridge connecting the charged moiety with the

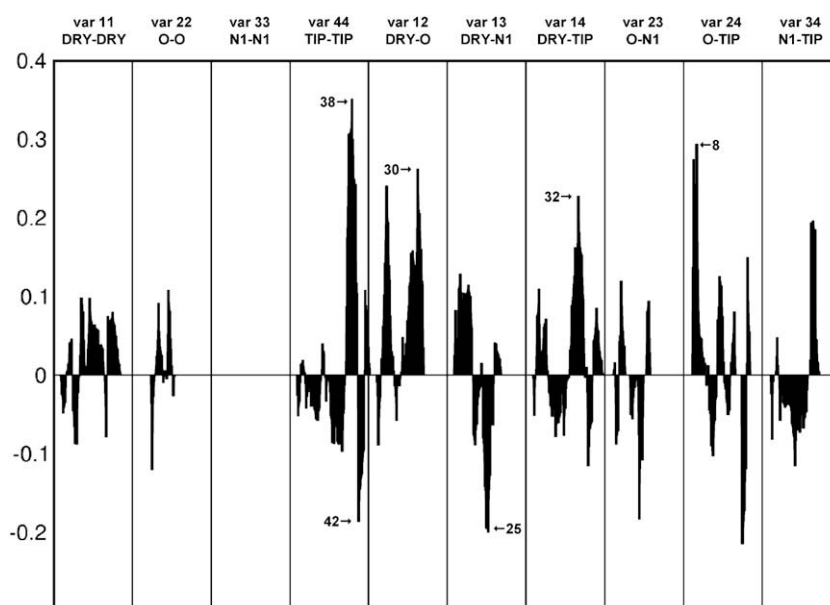


Fig. 5. PLS coefficients' plot for PB data as measured from (R)-A PLS models. Variables with highest and lowest coefficients are highlighted (see text).

lipophilic boundary of the studied compounds is not so crucial for ion channel blocking.

As already mentioned, GRIND descriptors translate at 3D level the inner relationships between regions defining the receptor

binding site and provide a chemically interpretable understanding of the measured affinity or potency. Therefore the aforementioned variables might suggest the optimal distance value (i.e. distance increasing molecule's potency) between certain pharmacophoric

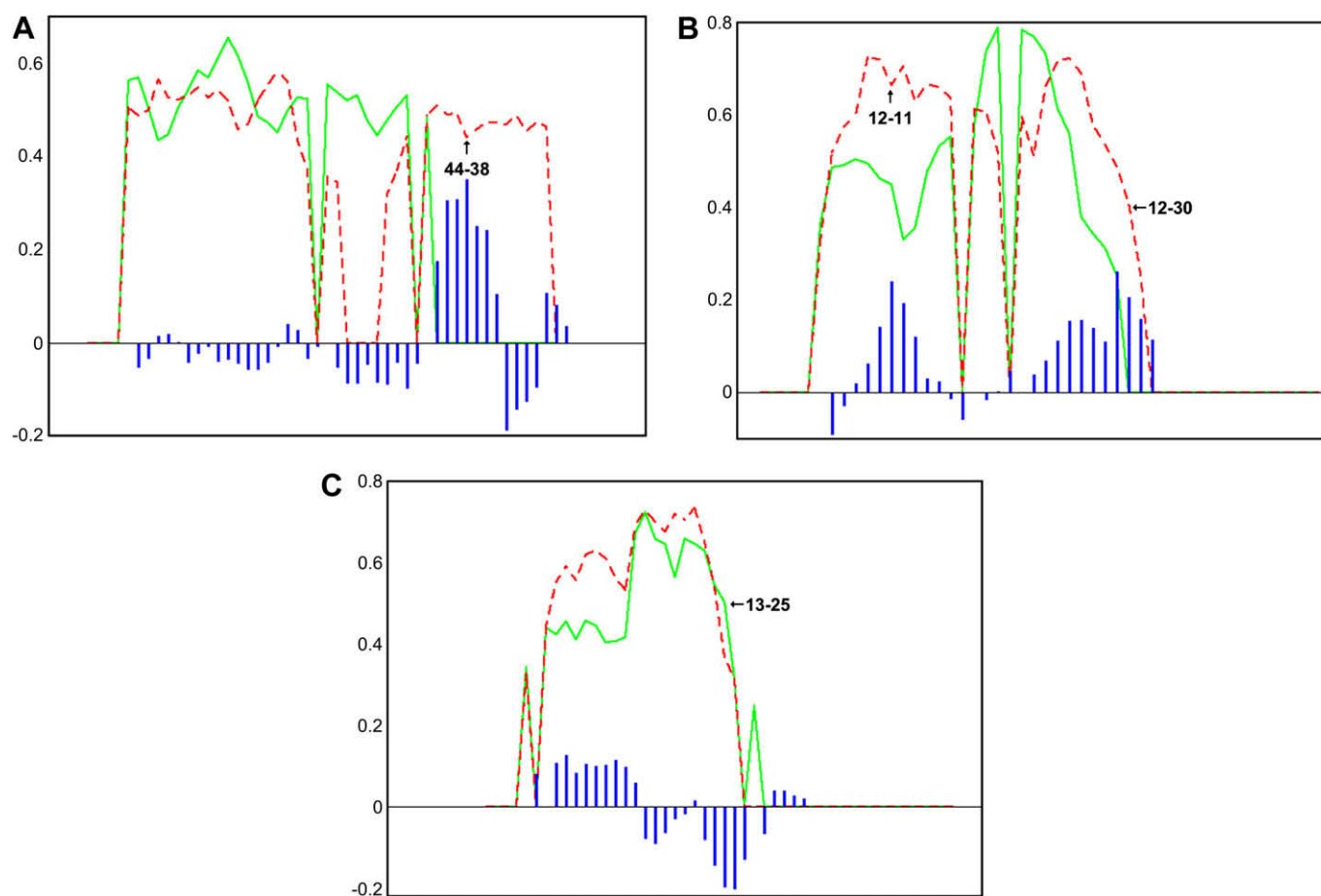


Fig. 6. TIP-TIP (top), DRY-O (middle), and DRY-N1 (bottom) correlograms for compounds (R)-8 (dashed line) and (R)-1 (solid line) as calculated from the PB chemometric analysis. Variables mentioned in the text are highlighted and bars represent PLS coefficients for the same variables.

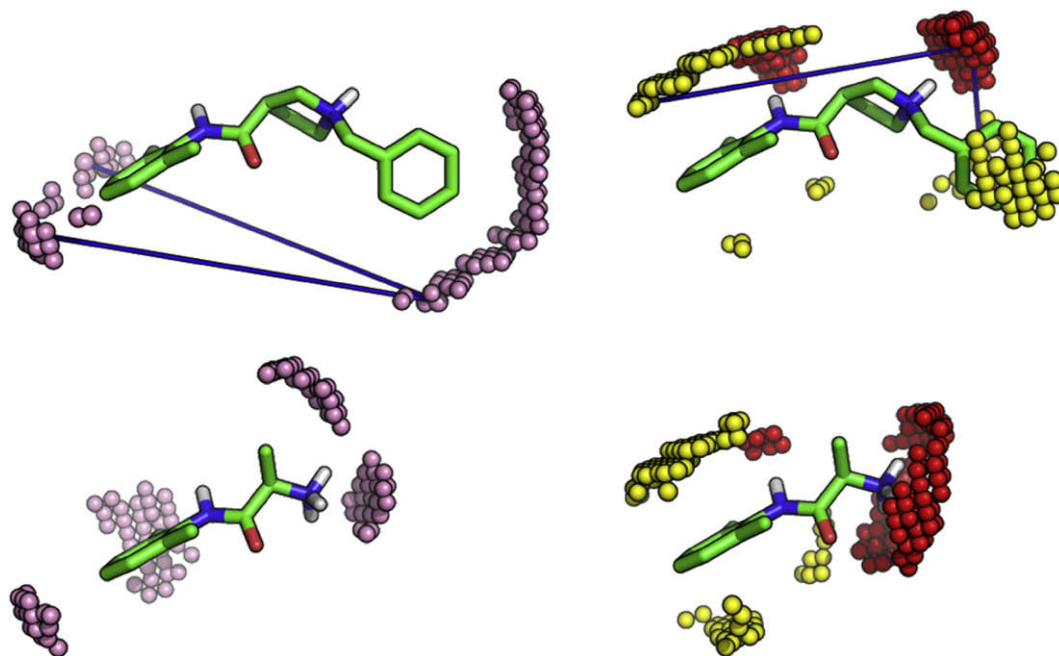


Fig. 7. Grid filtered fields for highly active (*R*)-**8** (top) and low active (*R*)-**1** (bottom) compounds for TIP–TIP (left) and DRY–O (right) descriptors (probe color code: pink TIP, yellow DRY, red O). Blue lines connect grid nodes affecting positively PB potency only present in the case of compound (*R*)-**8**.

groups within the studied data. These values are 15.2 Å for TIP–TIP, 4.4 and 12.0 Å for DRY–O interactions (see Fig. 6). A better understanding might be achieved by the graphical display of GRID filtered nodes relative to the mentioned interactions reported in Fig. 7. It can be noticed that fields have different extension and locations depending to the potency expressed by the different highly or low potent compounds.

In order to give a more robust support to 3D-QSAR results, the studied molecules were divided into a training set (TS), afterward used to predict PB value for molecules defining a prediction set (PS). Four VGSC blockers, namely (*R*)-**5**, (*R*)-**10**, (*S*)-**11** and (*S*)-**16** were scored, according to the PCA, as the most descriptive compounds and therefore excluded from the original data set. The remaining forty molecules were instead used to calculate a new 3D-QSAR model with the same procedure previously applied for the generation of PLS models reported in Table 2. Statistical indices of the TS were proved to be informative and significant, with high predictive power ($q^2 = 0.757$, $\text{ONC} = 5$) and valuable fitting to experimental data ($r^2 = 0.944$) and PLS coefficients highlighted same fields and variables already mentioned for model (*R*)-**A** as the most representative ones.

PB data predicted for PS molecules are reported in Table 3 where it can be seen that the potencies of all the compounds in the PS were predicted within 0.30 log units of their actual PB data with an average absolute error of 0.03 along a range of 2.08 units. Also these findings were quite gratifying.

PB chemometric analysis seems also to be in agreement with the 2D-QSAR equations since the relative influence of polar and hydrophobic molecular features is here confirmed by the type of GRIND descriptors with stronger weight on PLS models. This hypothesis is confirmed by the evidence that compounds with

a bigger volume and distance between molecule's edges show higher potency with respect to the ones bearing small substituents on the basic nitrogen. (cfr. compound **1** vs **8**, and **18** vs **19**).

Firstly, on the basis of this hypothesis it can be assessed that an increase in terms of shape and lipophilicity is mandatory to enhance PB activity; secondly, the charged moiety has to be placed at certain distance in order to properly space the two hydrophobic/aromatic ligand boundaries and the presence of an hydrogen atom on the basic nitrogen is essential.

4. Conclusions

In summary, significant 2D- and 3D-QSAR was carried out modeling the activity of ICBs on the inactive form of $\text{Na}_v1.4$. ALMOND chemometric analysis suggested a first pharmacophore hypothesis highlighting the structural need for an enhanced PB activity. In this view the synthesis and biological assay for newer TOC and MEX derivatives having a bigger shape and properly posed polar substituents is already ongoing. All these observations provide some predictions in order to design further sodium channel blockers potentially useful for pharmacological investigations such as channelopathies (e.g. myotonia).

5. Experimental section

5.1. X-ray

Crystal data for compound **8**: $\text{C}_{20}\text{H}_{24}\text{N}_2\text{O}$, $M_w = 308.41$, white plate, monoclinic, space group *Cc*, $a = 17.220(1)$ Å, $b = 25.709(2)$ Å, $c = 8.964(1)$ Å, and $\beta = 114.30(1)^\circ$, $V = 3616.9(5)$ Å³, $Z = 4$ ($Z' = 2$), $d_{\text{calcd}} = 1.133$ g cm^{−3}, Bruker AXS X8 APEX CCD system equipped with a four-circle Kappa goniometer and a 4 K CCD detector, radiation Mo K α , $\lambda = 0.71073$ Å, $2\theta_{\text{max}} = 60.00^\circ$, no. of measured reflections 21,151, no. of independent reflections 9373, no. of reflections included in the refinement 2906 ($I > 2\sigma(I)$), data reduction and unit cell refinement (package SAINT-IRIX [25]) integrated and corrected for Lorentz, polarization, and absorption effects using the program SADABS [26], $\mu = 0.070$ mm^{−1}, structure solution by direct methods and Fourier methods, SIR2004 [27] and SHELXL97

Table 3

PB potency data predicted by the training set.

Compound	PB (obs)	PB (pred)	PB (obs) – PB (pred)
(<i>R</i>)- 5	3.66	3.68	−0.02
(<i>R</i>)- 10	4.64	4.48	0.16
(<i>S</i>)- 11	5.52	5.76	−0.24
(<i>S</i>)- 16	4.64	4.66	−0.02

[28], no. of parameters 415, $R_1=0.0717$ and $wR_2=0.1311$ for observed reflections, calculations and molecular graphics were carried out using PARST97 [29], WinGX [30] and ORTEP-3 for Windows [31] packages. CCDC-668017 contains the supplementary crystallographic data for this paper. These data can be obtained online free of charge from the Cambridge Crystallographic Data Centre, 12 Union Road, Cambridge CB 2 1 EZ UK; fax +44 1223 336 033; or deposit@ccdc.cam.ac.uk.

5.2. Chemistry

5.2.1. Synthesis of (RS)-2-(benzylamino)-N-(2,6-dimethylphenyl)propanamide (**8**)

Compound **8** was prepared according to the literature procedure [14] starting from Tocainide. Yield: 63%; mp 87.6–88.2 °C (EtOAc); IR (CHCl₃): 3309, 3020, 2577, 2350, 1765, 1460, 1361, 1161, 974 cm⁻¹; ¹H NMR (300 MHz, CDCl₃): δ 8.7 (br s, 1H exchangeable with D₂O, NHCO), 7.5–7.0 (m, 8H, aromatic protons), 4.0 (m, 2H, CH₂Ph), 3.9–3.8 (m, 1H, $J=6.933$ Hz, CHCH₃), 2.3–2.1 (s, 6H, aromatic CH₃), 1.6–1.4 (m, 3H, $J=6.945$ Hz, CH₃CH). MS (70 eV) m/z (%) 282 (M⁺, 0.6), 134 (100), 91 (82). Anal. for C₁₈H₂₂N₂O·0.25H₂O calcd: C, 75.36; H, 7.91; N, 9.76; found: C, 75.66; H, 7.86; N, 9.57.

5.2.2. (S)-(-)-2-(Benzylamino)-N-(2,6-dimethylphenyl)propanamide (**8**)

$[\alpha]_D^{20} = -9.1$ (c 1, CHCl₃). Anal. for C₁₈H₂₂N₂O calcd: C, 76.56; H, 7.85; N, 9.92; found: C, 75.45; H, 7.73; N, 9.54.

5.2.3. (R)-(+)-2-(Benzylamino)-N-(2,6-dimethylphenyl)propanamide (**8**)

$[\alpha]_D^{20} = +10.1$ (c 1, CHCl₃). Anal. for C₁₈H₂₂N₂O·0.17H₂O calcd: C, 75.76; H, 7.89; N, 9.82; found: C, 76.01; H, 8.24; N, 9.92.

5.3. Computational

All the computations were carried out on a Linux workstation (Pentium IV 2.52 GHz). Figures are rendered with PYMOL (<http://www.pymol.org>).

Acknowledgements

The authors gratefully acknowledge Prof. Manolo Pastor (IMIM, Barcelona) for his kind collaboration and helpful discussion in preparing this manuscript and Prof. Ferdinando Scordari and Dr.

Ernesto Mesto (University of Bari) for the X-ray diffraction data collection.

References

- [1] R. Amir, C.E. Argoff, G.J. Bennett, T.R. Cummins, M.E. Durieux, P. Gerner, M.S. Gold, F. Porreca, G.R. Strichartz, J. Pain 7 (2006) 1–29.
- [2] A.L. Goldin, R.L. Barchi, J.H. Caldwell, F. Hofmann, J.R. Howe, J.C. Hunter, R.G. Kallen, G. Mandel, M.H. Meisler, Y.B. Netter, M. Noda, M.M. Tamkun, S.G. Waxman, J.N. Wood, W.A. Catterall, Neuron 28 (2000) 365–368.
- [3] A.L. Goldin, J. Exp. Biol. 205 (2002) 575–584.
- [4] S.Y. Wang, G.K. Wang, Proc. Natl. Acad. Sci. U.S.A. 95 (1998) 2653–2658.
- [5] S.Y. Wang, C. Nau, G.K. Wang, Biophys. J. 79 (2000) 1379–1387.
- [6] A.L. Goldin, Annu. Rev. Physiol. 63 (2001) 871–894.
- [7] A.L. Goldin, Curr. Opin. Neurobiol. 13 (2003) 284–290.
- [8] M. Muraglia, C. Franchini, F. Corbo, A. Scilimati, M.S. Sinicropi, A. De Luca, D.C. Camerino, V. Tortorella, J. Heterocycl. Chem. 44 (2007) 1099–1103.
- [9] C. Franchini, F. Corbo, G. Lentini, G. Bruno, A. Scilimati, V. Tortorella, C.D. Conte, A. De Luca, J. Med. Chem. 43 (2000) 3792–3798.
- [10] C. Franchini, A. Carocci, A. Catalano, M.M. Cavalluzzi, F. Corbo, G. Lentini, A. Scilimati, P. Tortorella, D.C. Camerino, A. De Luca, J. Med. Chem. 46 (2003) 5238–5248.
- [11] F. Corbo, C. Franchini, G. Lentini, M. Muraglia, C. Ghelardini, R. Matucci, N. Galeotti, E. Vivoli, V. Tortorella, J. Med. Chem. 50 (2007) 1907–1915.
- [12] G.M. Lipkind, H.A. Fozzard, Biochemistry 39 (2000) 8161–8170.
- [13] G.M. Lipkind, H.A. Fozzard, Mol. Pharmacol. 68 (2005) 1611–1622.
- [14] Y. Uozumi, K. Yasoshima, T. Miyachi, S. Nagai, Tetrahedron Lett. 42 (2001) 411–414.
- [15] H. Kubinyi, J. Med. Chem. 20 (1977) 652–659.
- [16] BILIN <<http://www.kubinyi.de/bilin-program.html>>.
- [17] ACD/LogP DB, Advanced Chemistry Development, Inc., Toronto, ON, Canada, 15 January, 2007. <www.acdlabs.com/logp>.
- [18] M. Pastor, G. Cruciani, I. Mclay, S. Pickett, S. Clementi, J. Med. Chem. 43 (2000) 3233–3243.
- [19] P.J. Goodford, J. Med. Chem. 28 (1985) 849–857.
- [20] ALMOND Version 330, Molecular Discovery Ltd., 4 Chandos Street, London W1A3BQ, 2002. <<http://www.moldiscovery.com>>.
- [21] G. Caron, G. Ermondi, J. Med. Chem. 50 (2007) 5039–5042.
- [22] C. McMartin, R.S. Bohacek, J. Comput. Aided Mol. Des. 11 (1997) 333–344.
- [23] C. Hansch, T. Fujita, J. Am. Chem. Soc. 86 (1964) 1616–1626.
- [24] A. Agarwal, P.P. Pearson, E.W. Taylor, H.B. Li, T. Dahlgren, M. Hersolf, Y. Yang, G. Lambert, D.L. Nelson, J.W. Regan, A.R. Martin, J. Med. Chem. 36 (1993) 4006–4014.
- [25] Bruker SAINT-IRIX, Bruker AXS Inc., Madison, Wisconsin, USA, 2003.
- [26] G.M. Sheldrick, SADABS Program for Empirical Absorption Correction of Area Detector Data, University of Göttingen, Germany, 1996.
- [27] M.C. Burla, M. Cavalli, B. Carrozzini, G. Cascarano, P. Giacovazzo, G. Polidori, G.R. Strichartz, J. Appl. Crystallogr. 36 (2003) 381–388.
- [28] G.M. Sheldrick, Programs for Crystal Structure Analysis (Release 97-2), Institut Anorg Chemie der Universität Tammanstrasse, 4 D-3400 Göttingen, Germany, 1998.
- [29] (a) M. Nardelli, Comput. Chem. 7 (1983) 95–97; (b) M. Nardelli, J. Appl. Crystallogr. 28 (1995) 659.
- [30] L.J. Farrugia, J. Appl. Crystallogr. 32 (1999) 837–838.
- [31] L.J. Farrugia, J. Appl. Crystallogr. 30 (1997) 565.